Fabrication and Characterization of TiO_2 doped Na-Tungstate (Heteropolyacid): Evaluation of Hall voltage across electrical conductor

Shivaprasad Chalawadi[1], SatyappaKalliguddi[1], Malatesh S. Pujar[2], Mallikarjunagouda B Patil[3], Rajashekhar F. Bhajantri[1*]

[1]*Department of Physics, Karnatak University, Dharwad-580003, Karnataka, India*

[2]*Department of Physics, KLE Dr. M. S. Sheshgiri College of Engineering and Technology, Belagavi-590008, Karnataka, India*

[3]*P. G. Department of Chemistry, Basaveshwar Science College, Bagalkot-587101, Karnataka, India*

Abstract: In this work, we report 0.1 to 3wt. % of the titanium oxide (TiO2) doped with Sodium-Tungstate using heteropolyacid new generation conducting material by sol-gel method. The prepared new samples were molded into circular discs and were assessed to measure the Hall current via Hall coefficient and electrical conductivity. Using the Hall effect method, the highest conductivity value is obtained as 1.531 to 2.654 S cm-1. Impedance spectroscopy is performed to know information about bulk and grain boundary resistance. The tailored material was further characterized by Powder X-ray diffraction (PXRD) to study the crystalline structure, Fourier transform infrared spectroscopy (FTIR) and Secondary electron microscopy (SEM) is performed to know about functional groups and material surface morphology respectively. The doped sample has an over stoichiometric range upon the undoped sample in terms of electronic transport properties. The contrastive analysis between doped and undoped samples allows some conclusions about the atomic and electronic transport properties, both at high and low temperatures.

Keywords- Nanoparticles, Heteropolyacid, FTIR, Hall Effect and Hall coefficient.

I. INTRODUCTION

Tungstates have numerous and fascinating properties which gained more interest in the various fields of scientific and industrial applications such as microwave, scintillation, optical modulation, magnetics and writing-reading-creasing devices, humidity sensors, optical fibers, photoluminescence materials, and photocatalysis. High thermal stability, semi-conductivity and interesting optical properties have placedphthalocyanine-based materials among the top attractive ones for modern technologies [1-5].
They are also used as component materials in the improvement of fuel cells such as electrolytes of a molten carbonate cell [6]. Nanocomposites-based studies on organic compounds give excellent performance because their structural modification has potential applications in thermal stability, conductivity, and optical properties. Iron-phthalocyanine is a p-type organic semiconductor metal-phthalocyanine(M-pc) that has high molecular symmetry, high conjugated 18- electrons, and a strong absorption band of light. These compounds have great applications in photovoltaic solar cells, light-emitting diodes, gas sensors, and transistors.

Silver tungstate (Ag_2WO_4) is an important inorganic semiconductor exhibiting unique optical, structural, and electrical properties that make it for diverse applications. The organic and inorganic nanocomposite materials also have ample applications in the field of catalysis and optoelectronics devices. [9].

Along with various nanomaterials, Sodium tungstate (Na_2WO_4) is one of the inorganic compounds. The tungsten compounds have general formula AWO_4 and B_2WO_4 (A, divalent cation; B, monovalent cation) crystallize structure depending upon the ionic radius of the cation element. Sodium tungstate Na_2WO_4 and molybdate Na_2MoO_4 crystals are isostructural, and they belong to the same class with the general formula $Na_2X_nO_{3n+1}$ (X= W, Mo). These materials have gotten more attention because they exhibit a rich

polymorphism. Sodium tungstate Na_2WO_4 is used for many applications such as the preparation of electrodes for electrolysis and as a fire retardant for fabrics [10].

Titanium dioxide TiO_2 is one of the most widely used transition metal oxide semiconductors due to its chemical stability and commercial availability at low cost, robust, and nontoxic nature. In the present work, we made nanocomposite pellets of Na_2WO_4 doped with TiO_2 nanoparticles at different weight percentages. The Hall Effect studies were done on the prepared samples through which their conductivity and mobility were calculated.

II. EXPIREMENTAL MATERIALS AND METHODS

Materials

Sodium Tungstate AR/ACS (Dihydrate)(LOBA Chemie) $Na_2WO_42H_2O$ Mw 329.86 was Used, Titanium(IV) isopropoxide (TTIP) Mw 284.22 (97%, Sigma-Aldrich, India), Cyclohexane (Cy) (Sigma-Aldrich, India), and Triton X-100 (TX) (Sigma-Aldrich, India) were used as precursor, solvent, and surfactant, respectively, without further purification, and distilled water was applied to initiate the hydrolysis

TiO_2 Nanoparticles Preparation

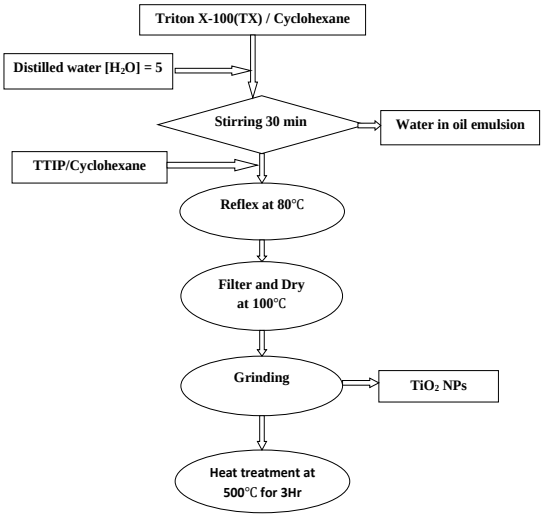

Fig. 1 The detailed synthesis route of TiO_2 nanoparticles

Titanium(IV) isopropoxide (TTIP) (ABCR, Germany), cyclohexane (Cy), and Triton X-100 (TX) (Sigma-Aldrich, USA) were used as precursor, solvent, and surfactant, respectively, without further purification, and distilled water was applied to initiate the hydrolysis. All the amounts of the reagents were kept fixed to the following values, in molar ratios: [H2O]/[TX]/[TTIP] 10/1/1, whereas cyclohexane volumes were evaluated from the ratio: [TTIP]/[Cy] 5.10^{-4} mol.mol^{-1}, as reported in the literature [8]

Figure 1 shows the schematic representation of the synthesis procedure. Firstly, the reverse micellar environment was prepared by the dissolution of TX in Cy at room temperature and stirring for 10 minutes and then the dropwise addition of stoichiometric amount of distilled water followed by a further 30 minutes stirring. In the next step, the solution of TTIP in Cy was added to the reverse micelle solution and immediately the powder formation occurred. All the obtained suspensions were left under stirring for 30 min before stopping the reaction (sample with no reflux) or starting the reflux step at 80°C for different times.[9]

Further step provided the removal of the micellar environment by adding to the suspensions a fixed volume of water/ethanol 1/1 solution and leaving them in a separation funnel until the complete separation between oil and aqueous phases occurred. The powders were filtered and washed 4 times with the same amount of water; a drying was performed on the powders at 100°C overnight. Finally, a fraction of all samples were taken for heat treatment at 500°C for 3hr in a static air oven. Figure 1 summarizes the steps for preparation of TiO_2 nanoparticles.[10]

Nanocomposite disc preparations: The hybrid Na-Tungstate doped with anatase phase of TiO_2 nanoparticles(0.1-3 wt.%) forms the new generation nano matrix and that produces a conducting material. The materials were prepared by the sol-gel method. The prepared materials were molded to the circular disc by using the hydraulic press.

Sample Preparation: The well-grounded composites of 1 gm Na-Tungstate and 0.1-3 wt. % of the TiO_2 nanoparticles. Both samples were mixed thoroughly in a mortar while grinding with the pestle. Once grinded well, place the mixtures onto the pellet die and close it with a lid. Place in a hydraulic press and apply pressure up to 7 tons for 10 minutes.

After this carefully remove the pressed sample from the die. The pressed disc is in circular disc form and has a very fine surface by appearance. Fig 2 below shows the actual molded samples are stored properly. The molded samples were mounted in a Hall Effect circuit carefully and are shown in Fig 3.

Fig.2. Circular disc shaped molded nanomatric samples

Fig. 3.The prepared sample mounted in the Hall Effect measurement circuit.

The prepared samples were given the name depending upon the amount of dopant i.e. TiO_2 in the main matrix and are tabulated as follows in Table I.

Table 1-The nomenclature of the prepared samples.

Sample Name	S-0	S-1	S-2	S-3	S-4	S-5
TiO_2 in Na-Tungstate (in wt.%)	0	0.1	0.5	1	2	3

III. CHARACTERIZATION AND MEASUREMENT

The structural characteristics were done by X-ray powder diffraction (XRD) method, Using RIGAKUX-ray diffractometer with Cu-Kα radiation (λ=1.5406˚A, X-ray tube voltage = 40 kV, and current 30 mA). The scan was taken in the 2θ range from at the rate of per minute. An infrared spectroscopic study is very important to confirm the presence of O–W–O and Ti-O-Ti groups and to determine their modes of vibration. The Fourier transform infrared (FTIR) spectrum of the nanocomposite sample was recorded by the FTIR spectrophotometer (Thermo Nicolet, Avatar 370) in the range 4000–400 cm $^{-1}$. The surface morphology of samples was analyzed with a scanning electron microscope (SEM) JEOL MODEL JSM-6390LV, operating at 5 kV.

HALL EFFECT MEASUREMENT: The Hall Effect measurement is basically depending on Lorentz force. When an electron moves perpendicular to an applied magnetic field, it feels a force acting on it which is normal in both directions, and moves as a reply to this force and the force affected by the internal electrical field. The Lorentz force is as follows,

$$F_{Lorentz} = q\left[E + \left(v\ X\ B\right)\right]$$

An illustration of the Hall Effect is given in Fig 4. A circular tablet-shaped nanocomposite sample in which charge is carried by the electrons. A current with constant flow ‘I’ flows across the circular tablet to which a uniform magnetic field ‘B’ is applied, which is directed into the screen, perpendicular to the current flow. Since the electrons are traveling through the applied magnetic field, they are subjected to an upward Lorentz force and so drift to the top of the conducting metallic bar at the same time as maintaining their horizontal motion. This leads to a build-up of the opposite charge i.e. negative charge on one side of the metallic bar and a positive charge on the other side of the metallic bar due to lack of electrons. This leads to a potential difference between two adjacent sides of the sample and which will be measured in the account of HallVoltage‘V_H’.

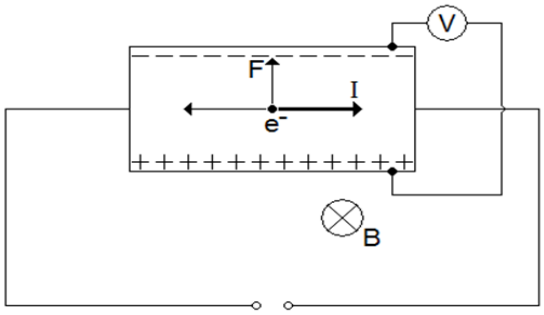

Fig. 4. The circuit diagram of Hall Effect in a circular disc.

This transverse voltage is the Hall voltage V_H and its magnitude is equal to IB/qnd, where I is the current, B is the magnetic field, where d is the sample thickness, and q (-1.602 x 10^{-19} C) is the elementary charge. In some cases, it is convenient to use layer or sheet density ($n_s = nd$) instead of bulk density. One then obtains the equation,

$$n_s = \frac{IB}{q|V_H|}$$

Thus, by measuring the Hall voltage V_H and from the known values of I, B, and q, one can determine the surface density n_s of charge carriers in composite material. If the measurement apparatus is set up as shown, the Hall voltage is negative for n-type semiconductors and positive for p-type semiconductors. The sheet resistance R_S of the semiconductor can be conveniently determined by the use of the Vander Pauw resistivity measurement technique. Since sheet resistance involves both sheet density and mobility, one can determine the Hall mobility from the equation,

$$\mu = \frac{|V_H|}{R_s IB} = \frac{1}{qn_s R_s}$$

The actual photograph of the Hall Effect experimental set up is shown in fig. 5.

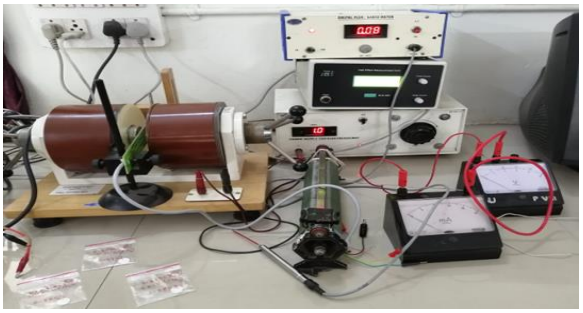

Fig.5. Actual photograph of the Hall Effect experimental set up

IV. RESULTS AND DISCUSSION

X-ray diffraction: XRD diffractogram for pure TiO_2, Na_2WO_4, and Na_2WO_4 doped with TiO_2 is indicated in Fig. 6.The diffraction peak of TiO_2 at an angle 2θ=18.5°, 21.03°, 25.8°, 27.0°,28.2°, 29.2°, 33.65°, 41.47°,44.3°,45.6° whereas characteristic peak Na_2WO_4 was obtained at angles 2θ=12.8°,14.8°, 16.7°, 20.9°, 21.1°, 24.6°, 27.0°, 33.5°,41.4°, 42.9°, 44.5°, 44.7°, and 45.7°.The XRD analysis was carried out in order to understand the crystalline and amorphous nature of the composite material.The Fig.6 (b) depicts the XRD patterns of different wt% of TiO_2 doped Na_2WO_4 composite. The intense peak in XRD patterns at 2θ = 12.82° and 28.2° is due crystalline nature of Na_2WO_4assigned to (1 2 0) plane (JCPDS # 00-053-0678) and TiO_2 plane (0 2 1) is assigned (JCPDS # 00-053-0619) respectively.The intensities of the Na_2WO_4 peaks are reduced while increasing the concentration of TiO_2 in composite matrices. The TiO_2 peak intensities decrease shows the interaction with the Na_2WO_4 in the composite.

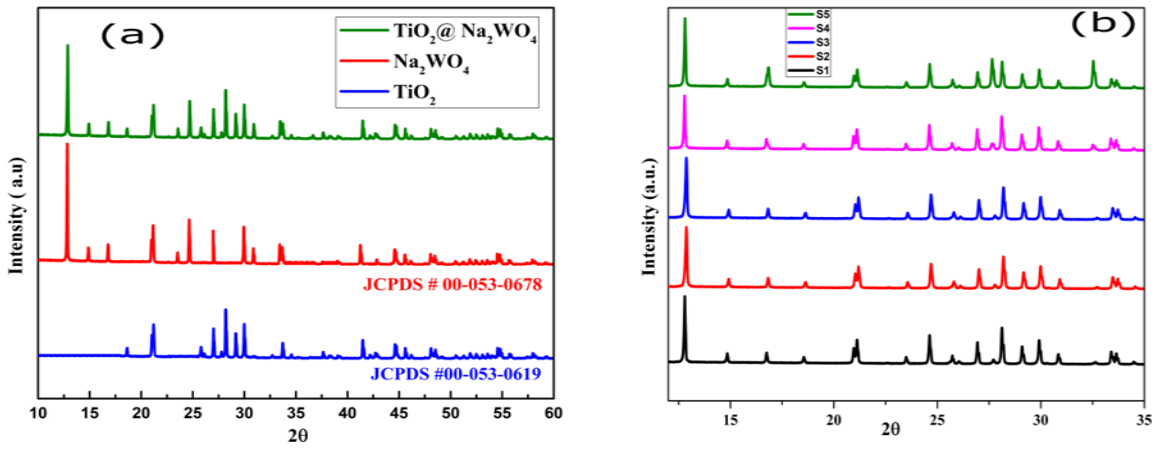

Fig.6.XRD spectra of (a)TiO_2,Na_2WO_4, and TiO_2@ Na_2WO_4 ,(b) different concentrations of TiO_2@ Na_2WO_4 S-1 to S-5 composites.

FTIR analysis: To further confirm and illuminate FTIR spectra were recorded for TiO_2 and TiO_2@ Na_2WO_4 composites in transmittance mode and illustrated in Fig. 7. The detailed labeling of the prominent peaks of TiO_2@ Na_2WO_4composites is summarized in Table III.It was reported that for TiO_2 the broad band from 1000-400 cm^{-1} region is to the Ti-O stretching and Ti-O-Ti bridging stretching modes.

The broad absorption band 450-800cm^{-1} is contributions of the antase Titania. For Na_2WO_4 observed band in the FTIR graph shows that 3373 and 1631.5 cm^{-1} region related to stretching and bending of O-H bond, 902.56 cm^{-1} band to stretching of O-O,883.27cm^{-1} for W=O,782.99,582.42 and 551 cm^{-1} bands to the stretching of O-W-O, Tungsten-Oxygen single bands bending vibration of O-W-O respectively. The composite bands changed its region due to doping observed 3265 cm^{-1}and 1673.98 cm^{-1}.For O-H stretching and bending vibration.929.56 cm^{-1},852.41 cm^{-1}, 686 cm^{-1} and 586.27 cm^{-1} strong peak of W=O, bonds are typical of tungstate anion W=O vibrations, Ti-O-Ti stretching and tungsten oxygen single band vibrations respectively.

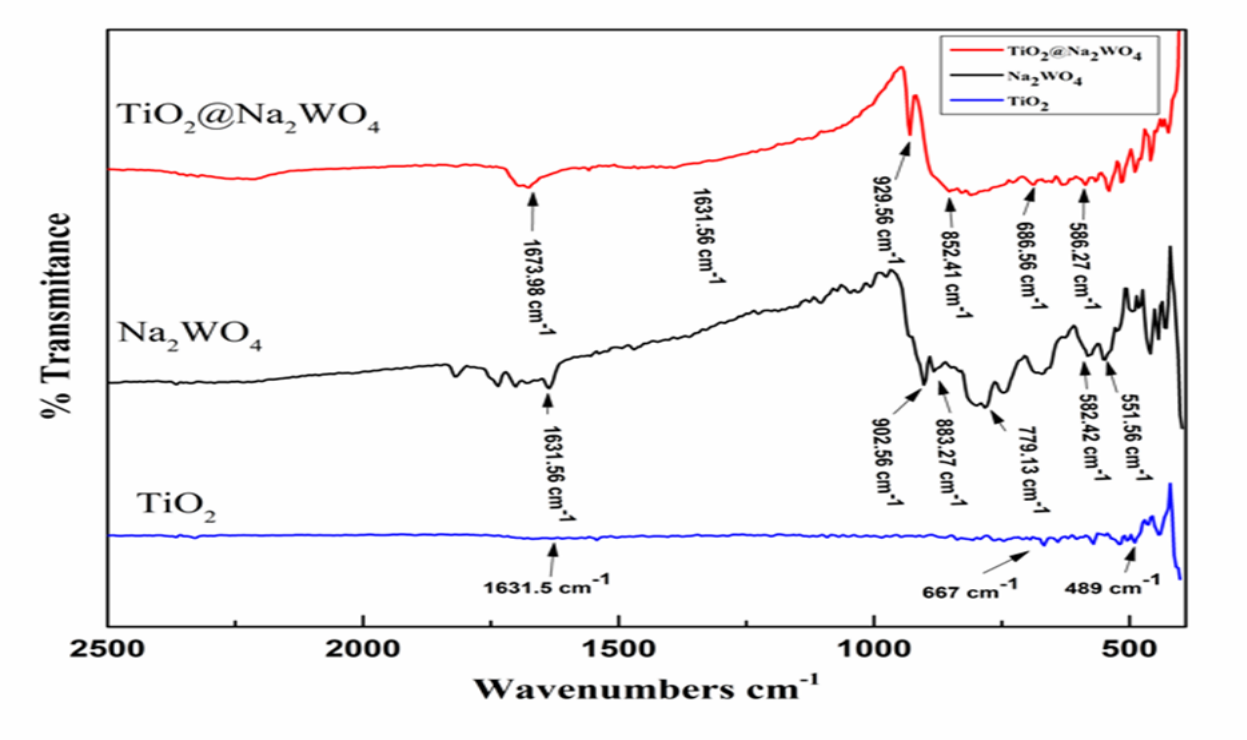

Fig.7.FTIR Spectra of TiO_2, Na_2WO_4 and TiO_2@ Na_2WO_4

Table 3The Characteristic FTIR bands of TiO_2 and TiO_2@ Na_2WO_4 composites Structures.Assignment of infrared bands for Na_2WO_4

Na_2WO_4 Wavenumbers(cm^{-1})	TiO_2 wavenumbers(cm^{-1})	TiO_2@ Na_2WO_4 wavenumbers(cm^{-1})	Attributions
3239.1	3287.7	3287.7	Stretching O-H (δ H_2O)
1631.5	1631.5	1673.98	Bending O-H(δ H_2O)
902.56	---	---	Stretching of O−O (i.e.υ O −O)
		929.56	Strong peak of W=O
883.27	---	852.41	υ W=O
779.13	---		Stretching of O−W−O (i.e. υ W −O)
	667	686.56	Stretching Ti−O−Ti
582.42	---		Tungsten Oxygen single bonds vibration
---	---	586.27	Tungsten Oxygen single bond vibration
551.56	---	---	Bending of O−W−O
---	489	---	Antase Titania

Table III: The Characteristic FTIR bands of TiO_2 and TiO_2@ Na_2WO_4 composites Structures. Assignment of infrared bands for Na_2WO_4

FESEM: SEM images of $TiO_2$and TiO_2@ Na_2WO_4 nanocomposite samples are shown in Fig. 8. The SEM image of TiO_2 shows orthorhombic elongated particles contains nanoholes between them with good aspect ratio. But, SEM image of TiO_2@ Na_2WO_4 nanocomposite shows a cluster of different shaped crystals such as block-like, rod-like crystals along with some spherical nanoparticles.

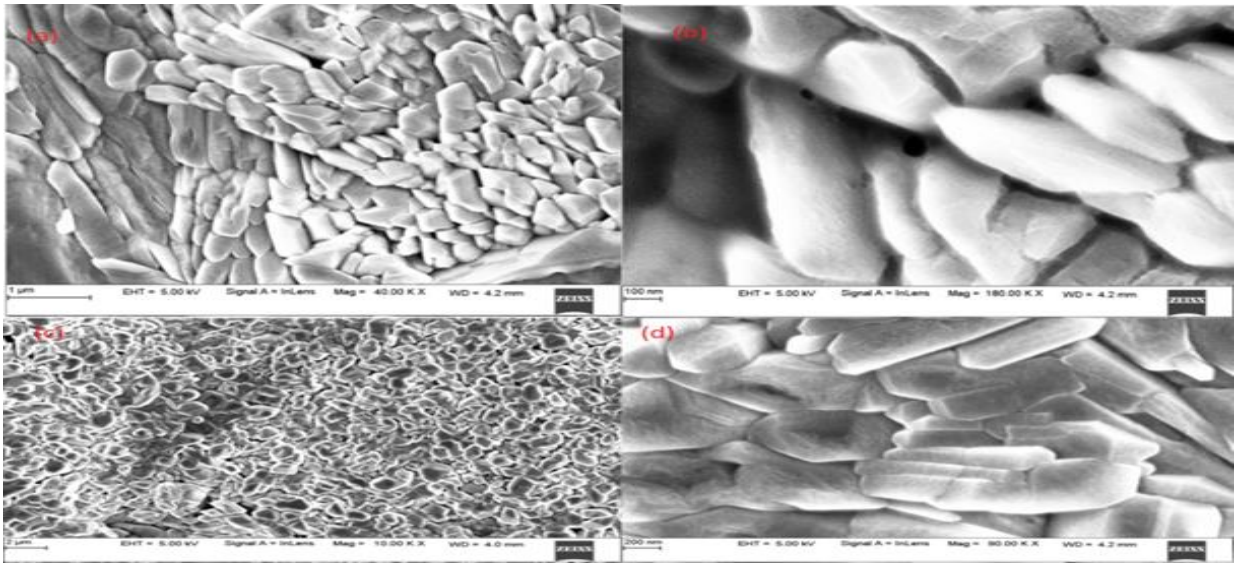

Fig.8.TheSEM images of (a) (b) TiO_2& (c) (d) TiO_2@ Na_2WO_4 nanocomposite sample.

Impedance Property Analysis: Impedance spectroscopy is one of the most important experimental techniques to find out the electrical properties of the sample and to resolve the contributions of various processes such as bulk, grain boundary and electrode effects in the specified frequency domain. This technique is useful to estimate the resistivity and capacitance and it analyses the charge transport processes in the grain–grain boundary of solids. The impedance spectroscopy of the different weight percent TiO_2doped with Na_2WO_4 nanocomposite were shown in fig. 9. The Nyquist plot of the samples shows the grain and grain boundaries with semicircles.

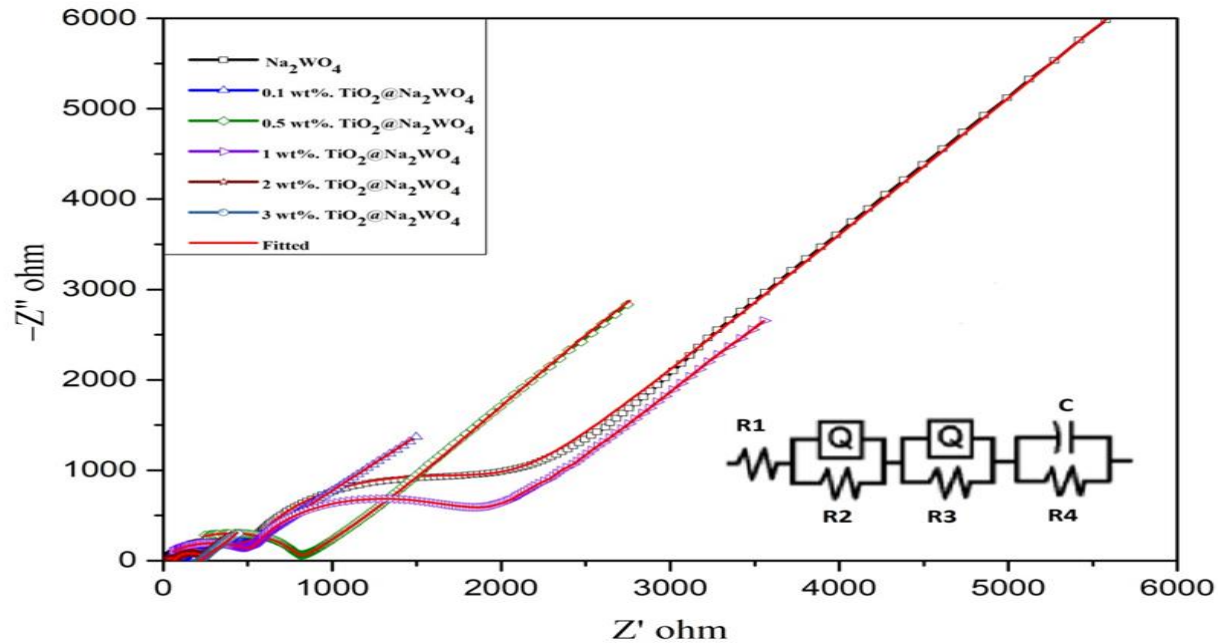

Fig.9.The impedance spectroscopy nyquiest plots of TiO2@ Na_2WO_4 nanocomposites with equivalent circuit.

From the impedance graph its clearly explains about the presence of grain boundaries in the composite samples. The impedance results were fitted using the equivalent circuit through ZSimpWin software. The resistance R and capacitance C values given in bellow table

Sample	R_b in Ω	σ_{ac}S cm^{-1}
S-0	724.3	6.3×10^{-3}
S-1	505.7	9.2×10^{-2}
S-2	510.4	9.5×10^{-2}
S-3	493.2	8.9×10^{-2}
S-4	490.1	8.9×10^{-2}
S-5	455.2	7.5×10^{-2}

Table-III: The values of resistance $R_b$and $R_{gb}$from impedance spectroscopy plot.

The ac conductivity increases with increase weight percentage of TiO_2.The linear line indicates the polarization of charges at the surface of stainless steel electrodes used to hold sample in the SS/Sample/SS.

Hall Effect measurement: The following data were obtained by the Hall Effect measurement,

Thin discs of prepared Sodium-tungstate doped with anatase phase TiO_2 with 0.1-3 wt. % using hydraulic press where used for the Hall Effect measurement.The Hall Effect measurements were performed to find parameters such as Hall coefficient, Carrier Density, Hall Mobility and Relaxation time as shown in Table III.

Our measurements showed p-type conductivity,the conductivity value (2.645 S/cm for S-2) is confining the good quality inter-grain contact of TiO_2 with Sodium-tungstate in the nanocomposite.

Sample	Hall coefficient in (cm^3/C)	Carrier Density *n* in (holes/cm^3)	Hall Mobility in ($\Omega^{-1}Cm^2$/C)	Relaxation Time in Sec	Conductivity in (S m^{-1})
S-0	1.2439	68173×10^{23}	0.1940×10^3	1.1033×10^{-9}	1.559
S-1	1.0215	72040×10^{23}	0.1944×10^3	1.1028×10^{-9}	1.903
S-2	0.7367	87890×10^{23}	0.19492×10^3	1.1034×10^{-9}	2.645
S-3	1.1378	88720×10^{23}	0.2793×10^3	1.1041×10^{-9}	2.455
S-4	1.929	91150×10^{23}	0.29402×10^3	1.1057×10^{-9}	2.464
S-5	2.123	99890×10^{23}	0.32522×10^3	1.1885×10^{-9}	1.531

Table-III: Hall Effect and Hall coefficient measurement.

The bulk carrier concentration of nanocomposite was 8.7890×10^{24} cm^3 which indicates the high concentration of charge carriers in the pellet. The mobility of the charge carrier depends on the thickness of the pellets. We measured on average mobility of $2.7328\ \Omega^{-1}m^2/C$ for the pellets.The Average relaxationtime $1.10463 \times 10^{-9} Sec$.

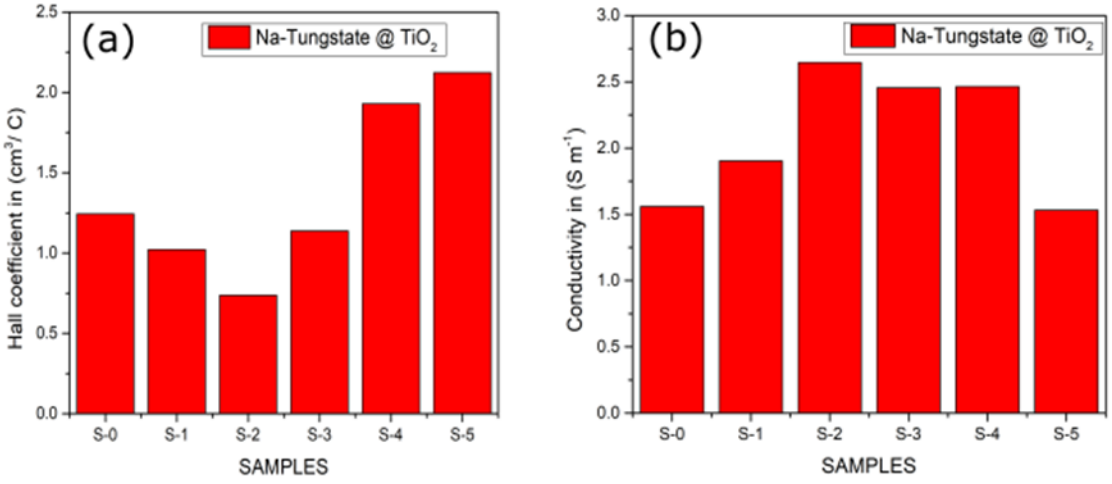

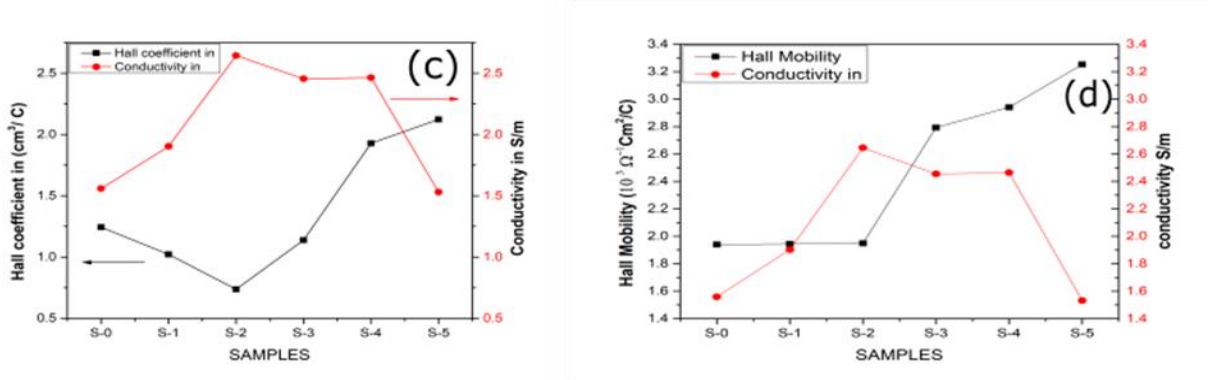

Fig.9.TheTiO_2@ Na_2WO_4 sample (a) Hall coefficient (b) Conductivity(c)Hall conductivity with hall coefficient (d) Hall Mobility with Conductivity.

From the Fig.8 (a) Hall coefficient R_H decreases with small rise in doping of TiO_2 from (0.1 to 0.5 wt. %) and increases at higher doping more than 1 wt. %, as shown graph. The (b) indicates the rise in conductivity for lower concentration is mainly due to the increase in carrier concentration, because of doping lower wt. % of TiO_2 may raise the free carrier.

For higher wt. % of TiO_2 the conductivity falls due to rapid increases in Hall coefficient as shown in graph (c).Hall mobility of slightly doped sample exceeds the corresponding value of conductivity at room temperature, while the specimen doped with more than 1wt% of $TiO_2$the conductivity as shown in (d) falls down although the carrier concentration increases in all cases [11-14]As a result, the heterostructures exhibit intriguing optical and electrical features as well as gas-sensing applications.

V. CONCLUSION

TiO_2@ Na_2WO_4composite samples are made into pellet by grinding in mortar and piston to make pallets and studied Hall Effect through which calculated conductivity 2.645S $m^{-1}$is observed for sample S-2.The conductivity mainly changes by the free carrier concentration *n* at room temperature.The XRD patterns confirm the TiO_2@ Na_2WO_4composite samples; by addition of $TiO_2$the intensity of the peak corresponding to Na_2WO_4 decreases indicates the interaction between compounds. The shift in the band is observed in FTIR of the nanocomposite indicates the interaction of compounds among themselves. The SEM images also support the impedance plot which conform the presence of grain boundary in the sample of nanocomposite. The heterostructures exhibits optical and electrical features as well as gas-sensing applications.

ACKNOWLEDGEMENTS

One of the authors Shivaprasad Chalawadi is grateful to the UGC-CSIR for providing JRF/SRF fellowship (519019/Dec 2016) (UGC award letter vide No. F. 16-6 (Dec. 2016)/2017(1406) dated 13.09.2017).Authors are also acknowledging the technical staff and Director of the USIC and SAIF (University Scientific Instrumentation centre& Sophisticated Analytical Instrument Facility), Karnatak University, Dharwad, Karnataka, India for the characterization techniques.Also thankful to B. V. V. Sangha, Bagalkot for providing experimental facilities.The authors also acknowledge the Science and Engineering ResearchBoard, Department of Science and Technology, Government of India,New Delhi, for the research project (SB/EMEQ-089/2013). The authors thank UGC, New Delhi, for providing financial assistance for the SAPCAS Phase-II program (F.530/9/CAS-II/2015(SAP-I). The authors arealso thankful to Karnataka State Higher Education Council, Govt. of Karnataka, for the RUSA1.0 grant (KSHEC/254/KUD/15–16/544) at KU. Dharwad.

CONFLICTS OF INTEREST

The Author here with declares that there is no conflict of interest with anyone regarding the publication of this paper.

REFERENCE

[1] Rajagopal S, Nataraj D, Khyzhun, O.Y.YahiaDjaoued, J.Robichaud, D.Mangalaraj, Hydrothermal synthesis and electronic properties

of $FeWO_4$ and $CoWO_4$ nanostructures, *J. Alloys Compds*,493,340,(2010) https://doi.org/10.1016/j.jallcom.2009.12.099.

[2] Maczka, M. Souza Filho, A.G. Paraguassu, W. Freire, P.T.C.Mendes Filho, J.Hanuza, Pressure-induced structural phase transitions and amorphization in selected molybdates andtungstates,*J.Prog.Mater.Sci*,57,1335(2012)https://doi.org/10.1016/j.pmatsci.2012.01.001

[3] Y Li, J Liu, X Huang, Synthesis and Visible-Light Photocatalytic Property of Bi2WO6 Hierarchical Octahedron-Like Structures, *Nanoscale Res. Lett*, 3,365,(2008) https://DOI 10.1007/s11671-008-9168-7

[4] M You, J Xu, Z Zhang,Y Zhou, Eu^{3+}-doped $CdWO_4$ phosphor for red-light emission: Hydrothermal preparation and blue light excitation, *Ceramics International*,40,(2014),16189. https://doi.org/10.1016/j.ceramint.2014.07.052

[5] R. Slota, G. Dyrda, W. Waclawek, Investigation of phthalocyanine crystals exposed to NO_2 ambient gas, *Polyhedron*, 21,677,(2002) https://doi.org/10.1016/S0277-5387(02)00832-X

[6] C.Luz-Lima, J.C.Batista, P.T.C.Freire, G.P. de Sousa, F.E.P dos Santos, J.Mendes Filho, B.C.Viana, G.D.Saraiva, Temperature-dependent Raman spectroscopy studies of phase transformations in the K_2WO_4 and the $MgMoO_4$, crystals*Vibrational Spectroscopy*,65,58, (2013) https://doi.org/10.1016/j.vibspec.2012.11.016

[7] J. Simon, J.J. Andre, Molecular Semiconductors: Photoelectrical Properties and Solar Cells, *Molecular Semiconductors Springer*, *Berlin*,pp. 237,274,(1985)10.1007/978-3-642-70012-5

[8] R. Zhang and L. Gao, Preparation of nanosized titania by hydrolysis of alkoxide titanium in micelles, *Materials Research Bulletin*,379,1659–1666,(2002) https://doi.org/10.1016/S0025-5408(02)00817-6

[9] Y. Sadaoka, T.A. Jones, W. Gopael, Fast NO_2 detection at room temperature with optimized lead phthalocyanine thin-film structures, *Sens. Actuat. B* 1,148, (1990) https://doi.org/10.1016/0925-4005(90)80191-2

[10] Sreedevi, A., Priyanka, K.P., Babitha, K.K. et al, Synthesis and characterization of silver tungstate/iron phthalocyanine nanocomposite for electronic applications, *The European Physical Journal B*,90,102,(2017), DOI: 10.1140/epjb/e2017-80149-9

[11] KuzminA, PuransJ, Local atomic and electronic structure of tungsten ions in AWO_4 crystals of scheelite and wolframite types, *RadiationMeasurements*,33,583–586, (2001) https://doi.org/10.1016/S1350-4487(01)00063-4

[12] M Itakura, N Niizeki, H Toyoda, H Iwasaki, Hall Effect and Thermoelectric Power in Semiconductive TiO_2,*Japanese Journal of Applied Physics*,6,311,(1967) DOI 10.1143/JJAP.6.311

[13] F Dkhilalli, S MegdicheBorchani, M Rasheed, R Barille, S Shihab, K Guidara, M Megdiche, Characterizations and morphology of sodium tungstate particles, *Royal Society open science*,5,(2018) https://doi.org/10.1098/rsos.172214

[14] H Shirakawa, A McDiarmid, A Heeger, Twenty-five years of conducting polymers *Chemical Communications*,7, 1–4,(2003), https://doi.org/10.1039/B210718J